Supporting Information

Hohl et al. 10.1073/pnas.1400485111

SI Methods

Mutagenesis. Cys-less TM287/288 (1) served as a template to introduce the $S498C^{TM287}$ and the $S520C^{TM288}$ mutations and to generate the double electron-electron resonance (DEER) mutants $S150C^{TM287}/T295C^{TM288}$, $T131C^{TM288}/S248C^{TM288}$, $T131C^{TM288}/S248C^{TM288}/D501A^{TM287}$, $T131C^{TM288}/S248C^{TM288}/D523A^{TM288}$, $S350C^{TM287}/K475C^{TM288}$, and $D460C^{TM287}/S363C^{TM288}$. Wild-type TM287/288 was used to make the mutants $D501A^{TM287}$ and $D523A^{TM288}$. The inactive LmrCD mutant $E587Q^{LmrD}$ carrying the Walker B glutamate-to-glutamine substitution in the consensus site was described (1). The D-loop mutants $D507A^{LmrC}$ and $D593A^{LmrD}$ were cloned into the *L. lactis* expression vector pNZ8048 by using the vector-backbone exchange (VBEx) cloning method (2).

Functional Analysis of TM287/288 and LmrCD Mutants. ATPase activity assays with detergent-purified TM287/288 were performed by determining liberated phosphate using molybdate/malachite green detection. All ATPase reactions were carried out in 20 mM Tris·HCl at pH 7.4, 150 mM NaCl, 10 mM $MgSO_4$, and 0.03% (wt/vol) β-DDM with three technical replicates for each ATP concentration. The ATPase assays shown in Fig. 3*C* and Fig. S5 were performed at 70 °C for 10 min. To detect phosphate, reaction solution (90 μL) was mixed with filtrated malachite green detection solution (160 μL) consisting of 10.5 mg/mL ammonium molybdate, 0.5 M H_2SO_4, 0.34 mg/mL malachite green, and 0.1% Triton X-100, and absorption was measured at 640 nm. ATP mixed with assay buffer was used for background subtraction. To identify the appropriate equation for nonlinear regression analysis, we performed an F-test analysis in which the Michaelis–Menten equation represented the null hypothesis and the Hill equation was the alternative hypothesis. For wild-type TM287/288, the analysis resulted in a P value of 0.0037 and an F value of 12.13, therefore clearly favoring the fit by using the Hill equation (SigmaPlot12.5). For the ATPase activity measurements with the $S498C^{TM287}/S520C^{TM288}$ mutant and the DEER mutants, the ATPase activity was measured at 50 °C in the presence of 1 mM ATP. DTT was added at 1 mM final concentration where indicated.

LmrCD-mediated transport of Hoechst 33342 and BCECF-AM was performed in *L. lactis* Δ*lmrA* Δ*lmrCD* (3) at 25 °C. Cells were grown in M17 medium incubated at 30 °C, and expression was induced at an OD_{600} of 0.4–0.6 with 5 ng/mL nisin A for 2 h. The fluorescence measurements were performed with cells diluted to an OD_{600} of 0.5 in 50 mM potassium phosphate at pH 7.0, 5 mM $MgSO_4$, and 0.5% glucose by using a Jobin-Yvon Fluoromax-4 spectro-fluorimeter (Horiba Scientific). Hoechst 33342 transport was measured at a final concentration of 0.5 μM. Excitation and emission wavelengths were set at 355 nm and 457 nm, with 4-nm slit widths. BCECF-AM transport was performed as described (4). Fluorescence measurements were independently carried out twice and repeated by using the same batch of cells. Representative results of one complete experimental dataset are shown.

Protein Crystallization. Production and purification of TM287/288 was performed as described (1). Crystals of TM287/288 in its nucleotide-free (apo) state were obtained by the vapor diffusion method in sitting drops at 20 °C against a reservoir containing 26% (wt/vol) polyethylene glycol (PEG) 400, 50 mM Na-cacodylate at pH 5.5, and 50 mM $CaCl_2$. The crystallization setups were performed in the presence of 2.5 mM ADP and 3 mM $MgCl_2$. Electron density for ADP was not observed in the solved structure. Crystals of TM287/288 were also obtained in the absence of nucleotides and $MgCl_2$ and grew against a reservoir containing 25% (wt/vol) PEG 400, 50 mM *N*-(2-acetamido)iminodiacetic acid at pH 6.5, and 50 mM Zn acetate. These crystals diffracted to 3.5 Å, and the resulting structure was indistinguishable to the high-resolution apo structure presented in this manuscript. The $S498C^{TM287}/S520C^{TM288}$ mutant was purified in the absence of reducing agents, which lead to an almost complete formation of the desired disulfide cross-link. Crystals were obtained in 32% (wt/vol) PEG 400, 50 mM Na-Acetate at pH 5, and 500 mM KCl. Although 2.5 mM AMP-PNP and 3 mM $MgCl_2$ were included for crystallization, electron density for the nucleotide was not observed.

Data Collection and Processing. All crystals were frozen without further cryoprotection. Diffraction data were collected at the protein crystallography beamline X06SA at the Swiss Light Source of the Paul Scherrer Institut and processed by using the program XDS (5). Apo TM287/288 was crystallized in the same space group as the previously solved AMP-PNP–bound TM287/288 (1). Diffraction data exhibited strong anisotropy and was therefore truncated by using the online anisotropy server of the University of California, Los Angeles using default settings (6), which lead to an improvement of the electron density map. Our previous AMP-PNP dataset (1) was reprocessed and cut at a resolution of 2.6 Å. The models were built in Coot (7) and refined by using PHENIX (8). Side-by-side comparison of constant parts of the apo and the nucleotide-bound structures allowed for an iterative improvement of both models. Data collection and refinement statistics are listed in Table S1. Superimpositions were performed with the CCP4 program Superpose.

Spin Labeling of the Cysteine Mutants for DEER. The cysteine mutants were Ni^{2+}-NTA–purified in the presence of 2 mM DTT. Before spin labeling, DTT was removed on a PD-10 column equilibrated with 20 mM Tris·HCl at pH 7.4, 150 mM NaCl, 0.03% *n*-dodecyl-β-D-maltopyranoside (β-DDM). MTSL [(1-oxyl-2,2,5,5-tetramethyl-Δ3-pyrroline-3-methyl) methanethiosulfonate, Toronto Research] was added in a 1:10 (cysteine to label) fold molar excess to the transporter sample and incubated at 4 °C overnight (for labeling efficiencies and ATPase activities, see Table S2). Excess of free spin label was removed by size exclusion chromatography in 20 mM Tris·HCl at pH 7.4, 150 mM NaCl, and 0.03% β-DDM on a Superdex-200 10/300 GL column. The spin-labeled pair $131^{TM288}/248^{TM288}$ was reconstituted into lipid membrane vesicles consisting of polar *E. coli* lipids and egg phosphatidylcholine mixed at a ratio of 3:1 as described (9).

DEER Analysis. Samples (40 μL final volume, protein concentration 30–40 μM) containing 10% (vol/vol) d8-glycerol (Sigma Aldrich) were inserted in 3-mm outer-diameter quartz tubes. To populate the AMP-PNP state, 2.5 mM AMP-PNP and 2.5 mM $MgCl_2$ were added before adding d8-glycerol. Tubes were preincubated at room temperature and then quickly frozen in a mixture of *n*-pentane and liquid nitrogen (–131 °C). The frozen tubes were inserted into the precooled home-made Q-band cavity (10, 11) at 50 K. DEER measurements were performed at Q-band frequencies (34–35 GHz) on a Bruker ELEXSYS E580 spectrometer equipped with a 200 W traveling-wave tube amplifier (Applied System Engineering). Dipolar time evolution data were acquired by using the four-pulse DEER experiment.

All pulses were set to 12 ns, and deuterium nuclear modulations were averaged by increasing the first interpulse delay by 16 ns for eight steps. The ELDOR frequency was set at the maximum of the echo-detected field swept spectrum, 100 MHz higher than the observer frequency (11). The background of the normalized DEER primary data [V(t)/V(0)] was fitted with the software DeerAnalysis2013 (12). Data were recorded for two different protein batches and found to be highly reproducible. The simulation of interspin distances on the X-ray structures was performed with the software MMM2013.2 (13) by using the MTSL rotamer library at 175 K. In Fig. 1*B*, the most populated rotamer at each spin-labeled site is presented (Table S3).

1. Hohl M, Briand C, Grütter MG, Seeger MA (2012) Crystal structure of a heterodimeric ABC transporter in its inward-facing conformation. *Nat Struct Mol Biol* 19(4):395–402.
2. Geertsma ER, Poolman B (2007) High-throughput cloning and expression in recalcitrant bacteria. *Nat Methods* 4(9):705–707.
3. Venter H, Velamakanni S, Balakrishnan L, van Veen HW (2008) On the energydependence of Hoechst 33342 transport by the ABC transporter LmrA. *Biochem Pharmacol* 75(4): 866–874.
4. Seeger MA, et al. (2012) Tuning the drug efflux activity of an ABC transporter *in vivo* by in vitro selected DARPin binders. *PLoS ONE* 7(6):e37845.
5. Kabsch W (2010) XDS. *Acta Crystallogr D Biol Crystallogr* 66(Pt 2):125–132.
6. Strong M, et al. (2006) Toward the structural genomics of complexes: Crystal structure of a PE/PPE protein complex from Mycobacterium tuberculosis. *Proc Natl Acad Sci USA* 103(21):8060–8065.
7. Emsley P, Lohkamp B, Scott WG, Cowtan K (2010) Features and development of Coot. *Acta Crystallogr D Biol Crystallogr* 66(Pt 4):486–501.
8. Adams PD, et al. (2010) PHENIX: A comprehensive Python-based system for macromolecular structure solution. *Acta Crystallogr D Biol Crystallogr* 66(Pt 2):213–221.
9. Geertsma ER, Nik Mahmood NA, Schuurman-Wolters GK, Poolman B (2008) Membrane reconstitution of ABC transporters and assays of translocator function. *Nat Protoc* 3(2):256–266.
10. Tschaggelar R, et al. (2009) Cryogenic 35GHz pulse ENDOR probehead accommodating large sample sizes: Performance and applications. *J Magn Reson* 200(1):81–87.
11. Polyhach Y, et al. (2012) High sensitivity and versatility of the DEER experiment on nitroxide radical pairs at Q-band frequencies. *Phys Chem Chem Phys* 14(30): 10762–10773.
12. Jeschke G, et al. (2006) DeerAnalysis2006 - a comprehensive software package for analyzing pulsed ELDOR data. *Appl Magn Reson* 30(3-4):473–498.
13. Polyhach Y, Bordignon E, Jeschke G (2011) Rotamer libraries of spin labelled cysteines for protein studies. *Phys Chem Chem Phys* 13(6):2356–2366.

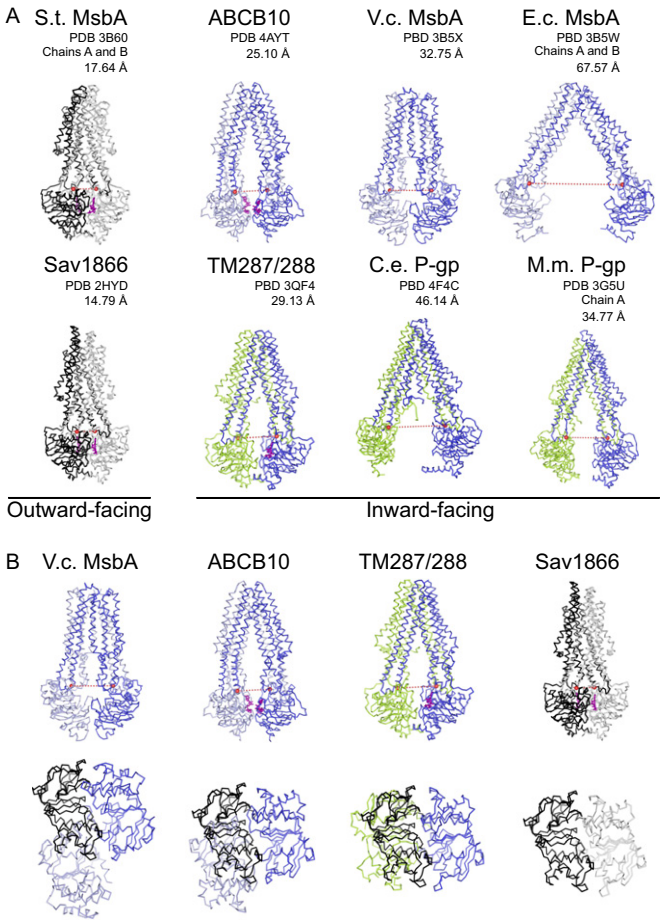

Fig. S1. Structural comparison of all crystallized ABC exporters. (*A*) The structures are shown from the side as ribbons. Inward-facing homodimers are colored dark blue and light blue. Inward-facing heterodimers are colored dark blue and green. Outward-facing homodimers are colored black and gray. The distances between the coupling helices (red dotted lines) were measured between C_α positions of residues corresponding to Gly201 in TM287 and Gly225 in TM288 (highlighted as red spheres). The distances are depicted next to the protein name and PDB ID code. Bound nucleotides are shown in purple (for TM287/288 one; for ABCB10, *Salmonella typhimurium* (S.t.) MsbA and Sav1866 two each). (*B*) Nucleotide binding domain (NBD) twisting analysis of TM287/288, ABCB10, and *Vibrio cholerae* (V.c.) MsbA. Chain A of the Sav1866 NBD dimer (gray) was taken as a reference for superimpositions. Displacement of the nonaligned chain is shown relative to chain B of the Sav1866 NBD dimer (black). For clarity, chain A of Sav1866 is omitted in the superimpositions. E.c., *Escherichia coli*; M.m., *Mus musculus*, C.e., *Caenorhabditis elegans*.

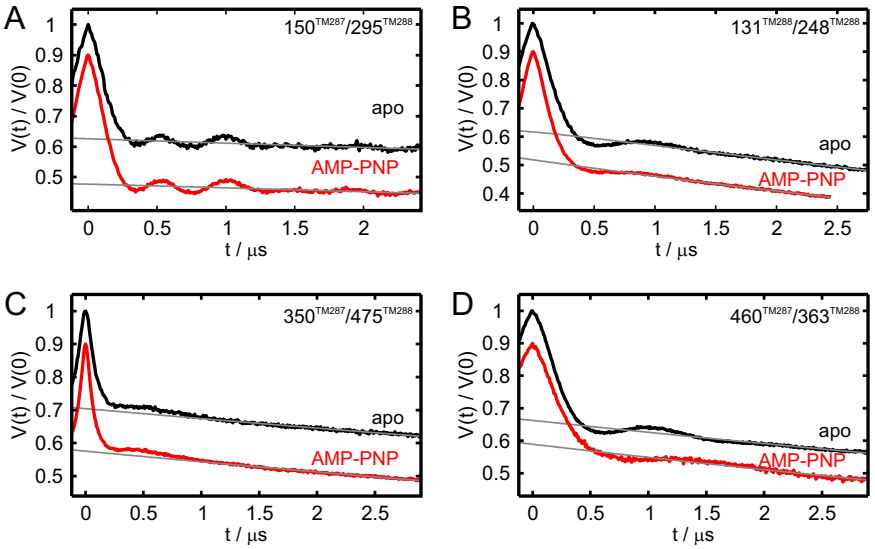

Fig. S2. Primary double electron-electron resonance (DEER) traces related to the data presented in Fig. 1. Primary Q-band DEER data $V(t)/V(0)$ (black and red lines) with the corresponding 3D background fits (gray lines) obtained with DeerAnalysis2013 are shown for the four pairs in the extracellular (*A*) and intracellular region of the exporter (*B–D*). All spin-labeled samples were measured after incubation at room temperature followed by flash freezing in cold liquid pentane in the presence (red) or absence (black) of adenosine 5′-(β,γ-imido)triphosphate (AMP-PNP) and $MgCl_2$.

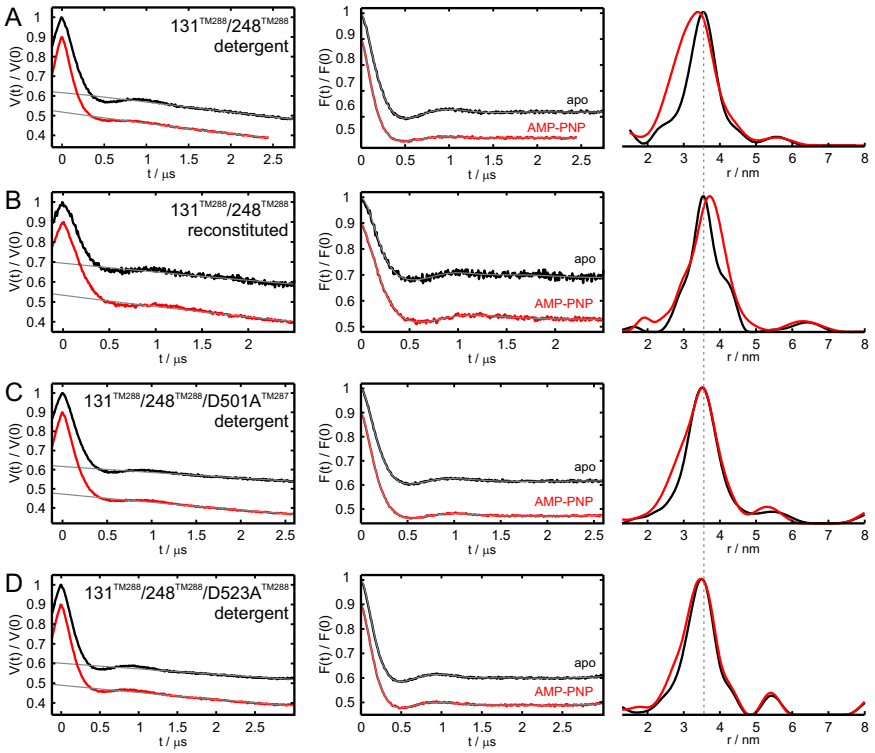

Fig. S3. Effects of protein reconstitution in liposomes and D-loop mutations on the distance in the intracellular spin-label pair $131^{TM288}/248^{TM288}$. Primary DEER data $V(t)/V(0)$ (black and red lines) with the corresponding background fits (gray lines) are shown in *Left* graphs. The background corrected Form factors $F(t)/F(0)$ (black and red lines) with the corresponding fits (gray lines) obtained with DeerAnalysis2013 are shown in *Center* graphs. Distance distributions obtained with a Tikhonov regularization parameter of 100 are shown in *Right* graphs. All spin-labeled pairs were measured after incubation at room temperature followed by flash freezing in cold liquid pentane in the presence (red) or absence (black) of AMP-PNP and $MgCl_2$. (*A*) Reference data in detergent solution identical to the ones shown in Fig. 1 and Fig. S2*B*. (*B*) DEER data obtained in proteoliposomes. (*C*) DEER data obtained for the $131^{TM288}/248^{TM288}$ pair containing the $D501A^{TM287}$ mutation. (*D*) DEER data obtained for the $131^{TM288}/248^{TM288}$ pair containing the $D523A^{TM288}$ mutation. A vertical dashed line guides the eye for the comparison between the different sets of distance distributions.

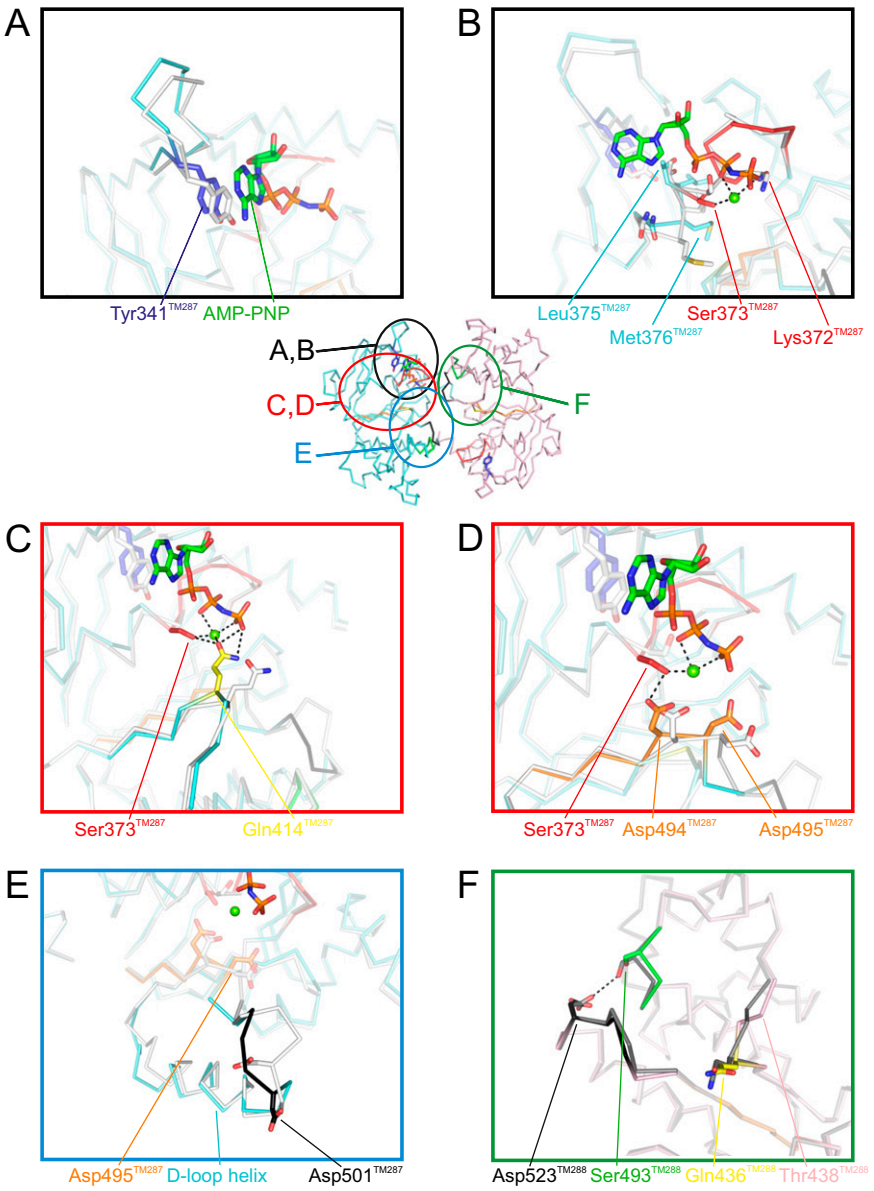

Fig. S4. Close-up views highlighting local differences seen between the nucleotide-bound (cyan/pink) and the apo structure (light gray/dark gray). The smaller picture in the second line is given as an overview. For clarity, conserved motifs are only colored in the AMP-PNP structure. AMP-PNP is shown as sticks in *A*–*E*, Mg^{2+} as a green sphere in *B*–*E* and hydrogen bonds and Mg^{2+} coordination as dashed lines. (*A*) Structural changes in the A-loop (blue) of NBD1. $Tyr341^{TM287}$ of the A-loop is highlighted as sticks. (*B*) Differences of the Walker A motif (red) in NBD1 and residues following Walker A. Walker A $Lys372^{TM287}$, $Ser373^{TM287}$, $Leu375^{TM287}$, and $Met376^{TM287}$ are shown as sticks. (*C*) Structural differences of the Q-loop (yellow) of NBD1. $Gln414^{TM287}$ (yellow) is shown in stick representation and is involved in Mg^{2+} coordination. (*D*) Deviations observed in the Walker B motif (orange) of NBD1. $Asp494^{TM287}$ and $Asp495^{TM287}$ of the degenerate site are shown as sticks. (*E*) Large conformational changes observed in the D-loop (black) of NBD1. $Asp501^{TM287}$ is highlighted as sticks. (*F*) Deviations seen in NBD2 associated with nucleotide binding to NBD1. The ABC signature motif is colored in green ($Ser493^{TM288}$), the D-loop in black ($Asp523^{TM288}$), and the Q-loop in yellow ($Gln436^{TM288}$).

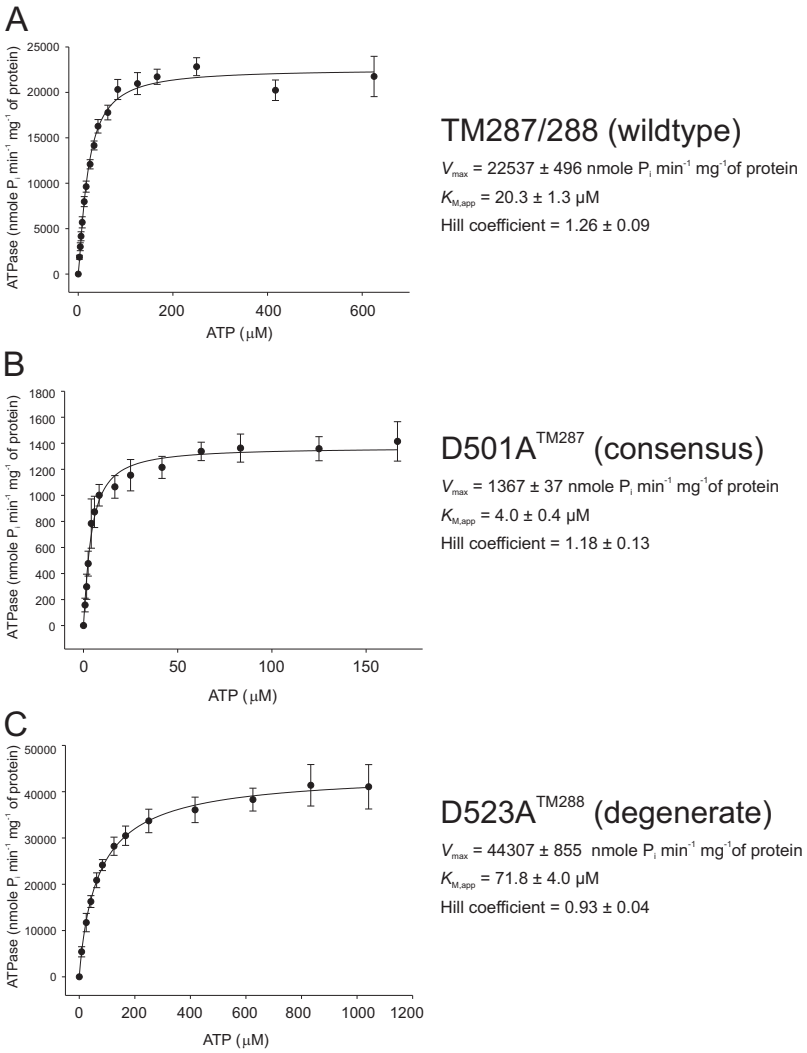

Fig. S5. ATPase activity measurements of the D-loop mutants of TM287/288. The data are identical to those shown in Fig. 3*C*. ATPase activities were determined at various ATP concentrations at 70 °C for wild-type TM287/288 (*A*), the consensus site D-loop mutant D501A^{TM287} (*B*), and the degenerate site D-loop mutant D523A^{TM288} (*C*). The error bars shown in the graphs correspond to the SD of three technical replicates. The data were fitted by nonlinear regression by using the Hill equation. V_{max}, $K_{M,app}$, and the Hill coefficient are indicated along with the SEMs obtained from nonlinear regression analysis.

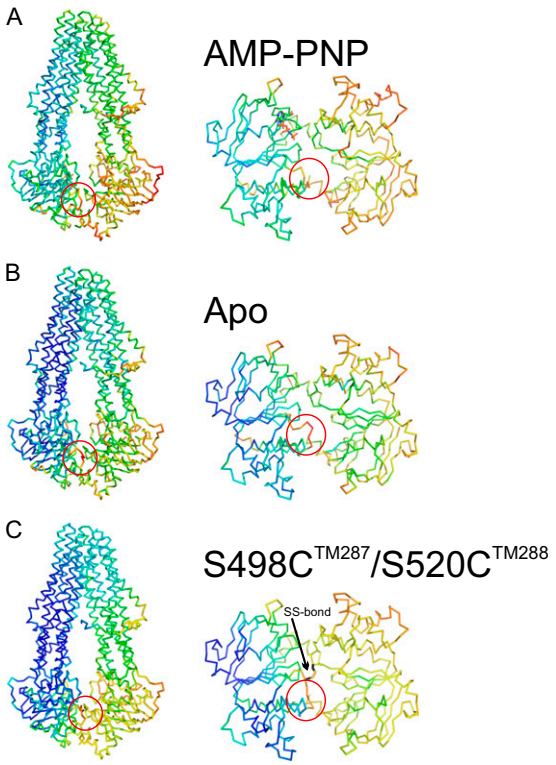

Fig. S6. B-factor analysis of the three TM287/288 structures. (*A*) B factors are shown for the nucleotide-bound structure, the full-length transporter viewed from the side (*Left*), and the NBDs from the top (*Right*). (*B* and *C*) Same analysis as in *A* for the apo structure (*B*) and the cross-linked S498C^{TM287}/S520C^{TM288}structure (*C*). The disulfide bond in *C* is highlighted as sticks. The D-loop of NBD1 is indicated with a red circle.

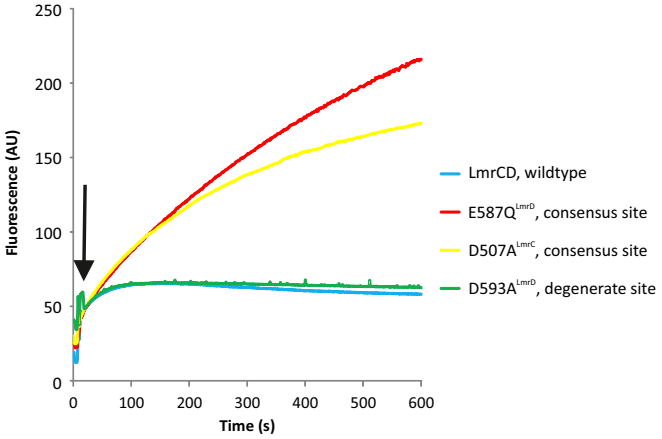

Fig. S7. Hoechst 33342 transport mediated by LmrCD D-loop mutants. Washed and preenergized *L. lactis* Δ*lmrA* Δ*lmrCD* cells expressing LmrCD wild type and mutants were supplemented with Hoechst 33342 (indicated by arrow) whose fluorescence signal increases upon binding to the membrane and chromosomal DNA. Active efflux mediated by LmrCD results in a slower increase of fluorescence. The inactive E587Q^{LmrD} mutant served as negative control.

Table S1. Data collection and refinement statistics

	Apo*	Apo† (PDB ID code 4Q4H)	AMP-PNP bound‡ (PDB ID code 4Q4A)	Cross-linked $S498C^{TM287}/S520C^{TM288}$ (PDB ID code 4Q4J)
Data collection				
Space group	C2	C2	C2	C2
Cell dimensions				
a, b, c, Å	214.64	214.64	216.33	216.67
	84.01	84.01	84.31	84.14
	114.11	114.11	115.78	113.46
α, β, γ, °	90.000	90.000	90.000	90.000
	93.268	93.268	91.923	93.325
	90.000	90.000	90.000	90.000
Resolution,§ Å	2.60 (2.67–2.60)	2.53 (2.59–2.53)	2.6 (2.67–2.60)	3.2 (3.28–3.20)
R_{merge}, %	5.3 (109.8)	5.3 (67.9)	6.2 (205.0)	5.8 (112.3)
I/σI	23.15 (1.32)	23.81 (1.66)	17.65 (1.36)	14.01 (1.58)
$CC_{1/2}$	100.0 (76.7)	—	100.0 (78.4)	99.9 (70.7)
Completeness, %	93.1 (64.6)	87.3 (25.6)	99.5 (99.4)	98.7 (99.6)
Redundancy	3.8 (2.5)	3.8 (2.0)	6.8 (7.0)	3.3 (3.5)
Refinement				
Resolution, Å		30–2.53	25–2.6	50–3.2
No. of reflections (work/test)		56,477/3,003	60,311/3,181	31,690/1,670
R_{work}/R_{free}		23.85/29.06	22.68/27.06	23.66/28.68
No. of atoms				
Protein		9,126	9,134	9,126
AMP-PNP		—	31	—
Mg^{2+}		—	1	—
Water		12	—	—
B factors				
Protein		109	123	106
Ligand		—	112	—
Ion		—	112	—
Water		67	—	—
rms deviations				
Bond lengths, Å		0.004	0.004	0.008
Bond angles, °		0.856	0.862	1.201

*Conventionally scaled data using XSCALE.
†Ellipsoidal truncation and anisotropy scaling was performed by using the University of California, Los Angeles Molecular Biology Institute—Diffraction Anisotropy Server (6).
‡Improved model of the previously deposited PDB ID code 3QF4.
§Highest resolution shell is shown in parenthesis.

Table S2. Simulated and measured DEER distances

Spin-labeled pair {Spin label efficiency}/[ATPase of labeled mutant in % of wt TM287/288]	Apo state (4Q4H)			AMP-PNP–bound state (4Q4A)		
	Experimental distance (σ), nm	Simulated distance (σ), nm	Delta, nm	Experimental distance (σ), nm	Simulated distance (σ), nm	Delta, nm
$131^{TM288}/248^{TM288}$ {80%}/[123%]	3.54 (0.84)	3.20 (0.46)	0.34	3.39 (0.87)	3.45 (0.48)	−0.06
$131^{TM288}/248^{TM288}$ in liposomes {100%}/[n.d.]	3.74 (0.85)		0.54	3.75 (0.92)		0.30
$131^{TM288}/248^{TM288}$ $D501A^{TM287}$ {90%}/[n.d.]	3.66 (0.91)		0.46	3.57 (0.92)		0.12
$131^{TM288}/248^{TM288}$ $D523A^{TM288}$ {100%}/[n.d.]	3.61 (0.90)		0.41	3.55 (0.91)		0.10
$150^{TM287}/295^{TM288}$ {100%}/[92%]	3.32 (0.94)	3.22 (0.40)	0.10	3.31 (0.92)	3.26 (0.33)	0.05
$350^{TM287}/475^{TM288}$ {65%}/[165%]	3.04 (1.13)	2.77 (0.36)	0.27	2.82 (1.10)	2.74 (0.36)	0.08
$460^{TM287}/363^{TM288}$ {70%}/[192%]	3.88 (0.92)	3.40 (0.43)	0.48	4.00 (0.94)	3.61 (0.33)	0.39

Comparison between mean experimental distances and those simulated on the two crystal structures. All distances were measured by using detergent-solubilized transporters, unless otherwise stated. The mean distances and the SD (σ) of the distributions are presented as obtained from DeerAnalysis2013 (12) in the range 1.5–8 nm (experimental data) or from MMM2013.2 in the same range (13) (simulated data). The difference between experimental and simulated mean distances is shown (Delta).

Table S3. Spin-labeled rotamers and partition function

	Apo state (4Q4H)		AMP-PNP–bound state (4Q4A)	
Spin-labeled site	No. of rotamers	Partition function	No. of rotamers	Partition function
131^{TM288}	66	0.83	82	0.87
248^{TM288}	62	0.89	76	0.96
150^{TM287}	93	2.55	84	1.67
295^{TM288}	6	0.19	8	0.19
350^{TM287}	80	2.39	58	2.06
475^{TM288}	95	1.17	86	0.88
460^{TM287}	127	1.19	120	1.04
363^{TM288}	25	0.32	30	0.65

Values were calculated with the software MMM2013.2 (13).

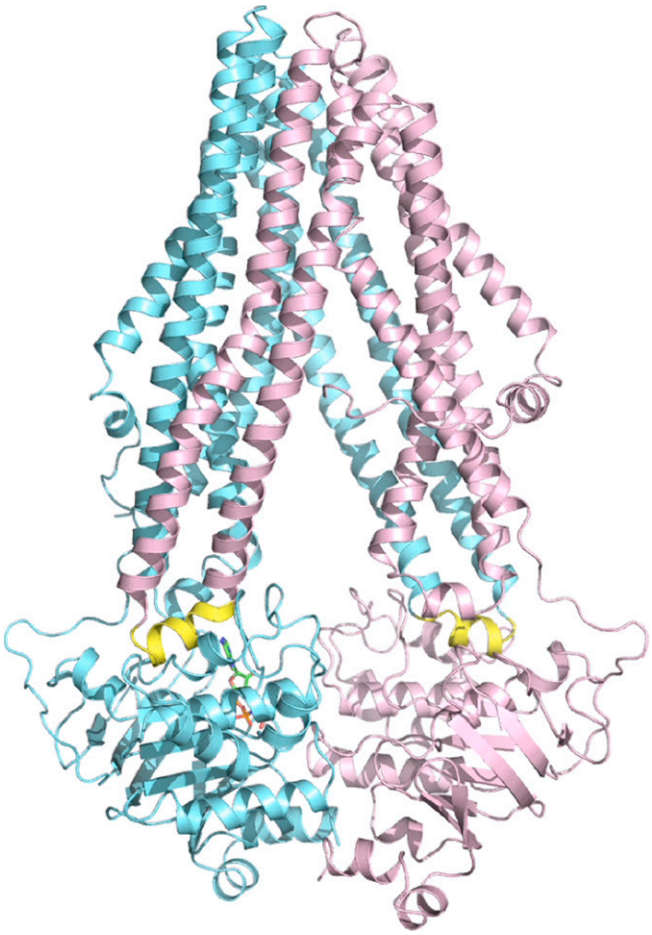

Movie S1. Morph between the apo and AMP-PNP–bound structures of TM287/288. Shown are the NBDs viewed from the top. Residues of the D-loops and the Walker B motifs, which are important for cross-communication between the degenerate and the consensus site are depicted as sticks and labeled. AMP-PNP is shown as sticks. The coupling helices of the TMDs are shown in yellow.

Movie S1